Molecular Vision 2016; 22:1198-1212 <http://www.molvis.org/molvis/v22/1198>
Received 27 January 2016 | Accepted 10 October 2016 | Published 12 October 2016

Deficient glucose and glutamine metabolism in *Aralar/AGC1/Slc25a12* knockout mice contributes to altered visual function

Laura Contreras,[1] Laura Ramirez,[2] Jianhai Du,[3,4] James B. Hurley,[3,4] Jorgina Satrústegui,[1] Pedro de la Villa[2]

[1]Centro de Biología Molecular Severo Ochoa CSIC-UAM, CI.B.E.R. de Enfermedades Raras, Instituto de Investigación Sanitaria Fundación Jiménez Díaz, Universidad Autónoma de Madrid, Madrid, Spain; [2]Department of Systems Biology, University of Alcalá, Alcalá de Henares, Spain.; [3]Department of Biochemistry, University of Washington, Seattle, WA.; [4]Department of Ophthalmology, University of Washington, Seattle, WA.

Purpose: To characterize the vision phenotype of mice lacking *Aralar/AGC1/Slc25a12*, the mitochondrial aspartate-glutamate carrier mutated in global cerebral hypomyelination (OMIM 612949).
Methods: We tested overnight dark-adapted control and aralar-deficient mice for the standard full electroretinogram (ERG) response. The metabolic stress of dark-adaptation was reduced by 5 min illumination after which the ERG response was monitored in darkness. We used the electrical response to two identical saturating light flashes (paired-flash stimulation) to isolate the inner retina and photoreceptor responses. Retinal morphology was examined with hematoxylin and eosin staining, immunohistochemistry of antibodies against retinal cells, and 4',6-diamidino-2-phenylindole (DAPI) labeling.
Results: Aralar plays a pivotal role in retina metabolism as aralar provides de novo synthesis pathway for glutamine, protects glutamate from oxidation, and is required for efficient glucose oxidative metabolism. Aralar-deficient mice are not blind as their retinas have light-evoked activity. However, we report an approximate 50% decrease in the ERG amplitude response in the light-evoked activity of dark-adapted retinas from aralar-deficient mice, in spite of normal retina histology. The defective response is partly reversed by exposure to a brief illumination period, which lowers the metabolic stress of dark-adaptation. The metabolic stress and ERG alteration takes place primarily in photoreceptors, but the response to two flashes applied in fast succession also revealed an alteration in synaptic transmission consistent with an imbalance of glutamate and an energy deficit in the inner retina neurons.
Conclusions: We propose that compromised glucose oxidation and altered glutamine and glutamate metabolism in the absence of aralar are responsible for the phenotype reported.

The retina, the neuronal tissue responsible for visual function, has one of the highest energetic requirements of the human body [1,2]. The retina is composed of several types of neurons ordered in layers. The photoreceptors, located in the outer retina, sense light and initiate the phototransduction cascade responsible for visual output [3]. Of the cells in the retina, photoreceptors have the greatest energy demand [4,5].

Retinal metabolism is highly glycolytic, with 80–96% of consumed glucose transformed to lactate [4,6]. However, because the yield of ATP from oxidation is much higher than that from glycolysis, mitochondria make a substantial contribution to overall energy production in the retina [7], especially in dark-adapted retinas when energy consumption by photoreceptors increases relative to light-adapted retinas [7-10]. In the dark, a continuous Na^+ influx through cGMP-gated channels generates the "dark current," which is opposed by sustained operation of Na^+/K^+ ATPase pumps in photoreceptors (Figure 1A). Light initiates the phototransduction cascade, which ultimately diminishes cGMP levels and closes the channels, slowing the dark current and diminishing the energetic burden. Thus, ion pumps are more active in the dark-adapted retina than in the light-adapted retina explaining the need for increased glucose oxidation in darkness [5,8,11-17]. The importance of glucose metabolism for photoreceptor activity is supported by the reduction in the electroretinogram (ERG) response amplitude when glucose metabolism is compromised [6,18-23].

Aralar/AGC1/Slc25a12 is the neuronal isoform of the mitochondrial aspartate-glutamate carrier (AGC), a critical component of the malate-aspartate shuttle (MAS) [24,25] (Figure 1B). Glucose oxidative metabolism requires NAD^+ regeneration from NADH produced in glycolysis mainly by the activity of the MAS [25]. In the absence of MAS activity, pyruvate produced in glycolysis will turn into lactate instead of proceeding to mitochondria for full oxidation. Consistent with the absence of MAS activity in aralar-deficient mice, cultures of cortical neurons from aralar-deficient mice have a 12-fold increase in the lactate to pyruvate ratio [26] and

Correspondence to: Laura Contreras, Centro de Biología Molecular Severo Ochoa CSIC-UAM, C/ Nicolás Cabrera, 1, 28049 Campus Cantoblanco, Univ. Autónoma de Madrid, Madrid, Spain; Phone: +34 91 196 4651; FAX: +34 91 196 4420; email: lcontreras@cbm.csic.es

46% slower glucose-fueled respiration [27] compared with their control counterparts. Furthermore, Ca^{2+} activation of the aralar-MAS pathway [28-30] is necessary to enhance pyruvate entry into mitochondria and to stimulate respiration in response to workload increases [27]. In addition to a role in glucose metabolism, aralar is important in the glutamine and glutamate balance in the brain. De novo synthesis of glutamine in astrocytes requires neuronal aspartate to act as an NH_4-group donor [26]. Aralar constitutes the main pathway by which aspartate leaves neuronal mitochondria, where it is synthesized in the brain [25], and therefore, aspartate and glutamine levels are diminished in the brains of aralar-deficient mice [26,31].

Aralar is highly expressed in photoreceptors of the outer retina and in all neurons of the inner retina. However, aralar is absent from Müller glial cells [32-34]. We have reported a decrease in glucose oxidation in aralar-deficient retinas measured as ^{13}C label incorporation into Krebs cycle intermediates and increased lactate to pyruvate ratios [35,36]. Furthermore, similar to de novo glutamine synthesis in the brain [26], the retina can use photoreceptor-derived aspartate as a glutamine precursor in Müller cells [32,33]. Consistent

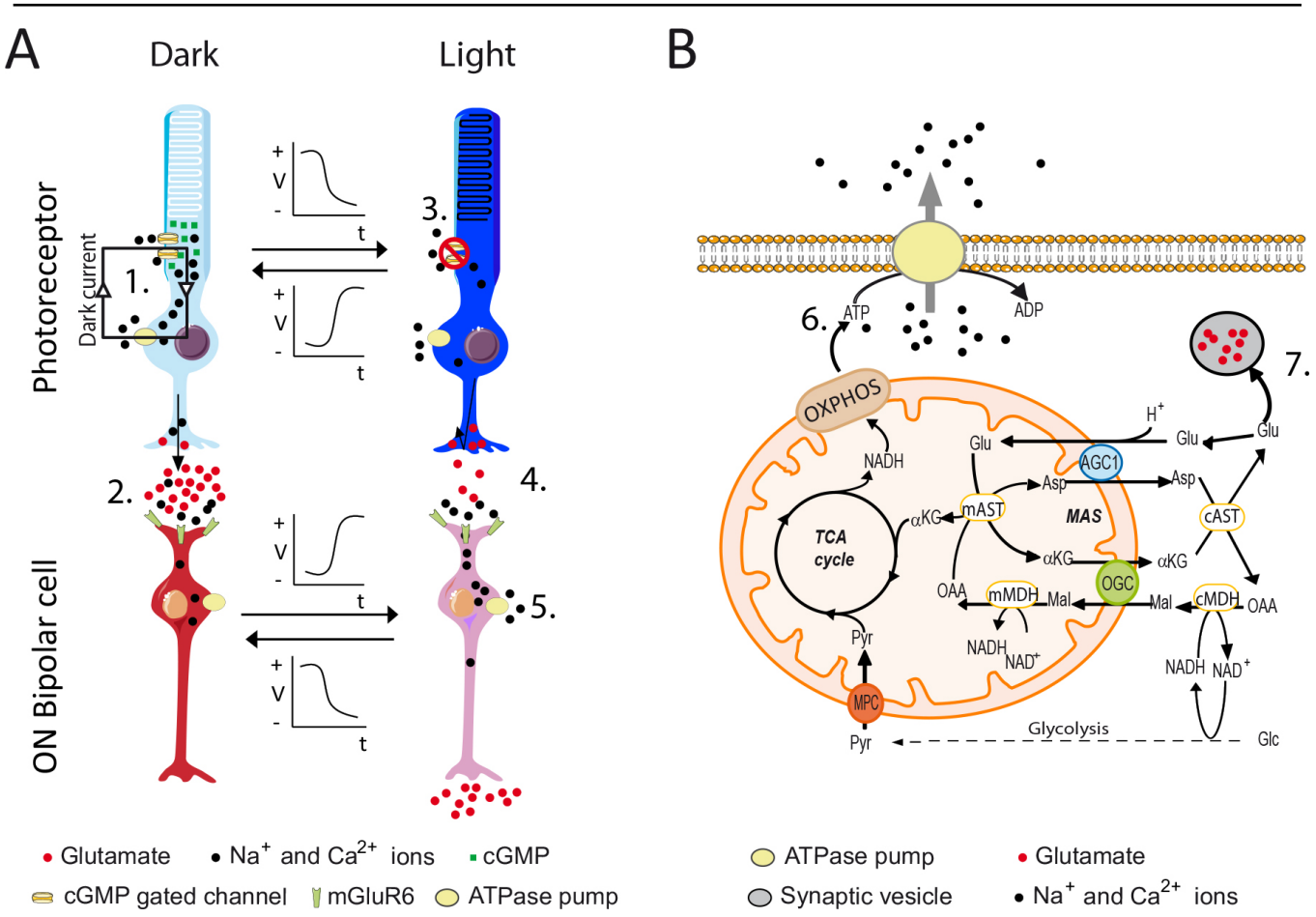

Figure 1. Metabolic requirements of the retina. **A**: In darkness, the elevated concentration of cGMP keeps the Na^+ and Ca^{2+} channels open, and the Na^+ inflow is counterbalanced by Na^+/K^+ pumps with high ATP expenditure to maintain the dark current (1). The photoreceptor is depolarized (light blue) and releases glutamate (2), which needs to be actively sequestered back and protected from oxidation. Light activates the phototransduction cascade decreasing cGMP levels, which closes the Na^+ and Ca^{2+} channel, reduces the dark current and ATP demand (3), and hyperpolarizes the photoreceptor (dark blue), decreasing glutamate release (4). In the darkness, the high glutamate level in the synapse keeps the ON bipolar cells polarized (dark red), whereas after light the ON bipolar cells become depolarized (light red) and will increase their energy requirement to fuel the ion pumps (5). **B**: Role of aralar in retinal metabolism. Aralar, as part of the malate-aspartate shuttle (MAS), is required for efficient ATP generation by glucose oxidative metabolism. The ATP (6) generated is necessary to fuel the ion pumps of the photoreceptors (dark) and the ON bipolar cells (light). Aralar also participates in the protection of glutamate from oxidation to serve as a neurotransmitter by photoreceptors (7). αKG, α-ketoglutarate; AGC1, aspartate-glutamate carrier; Asp, aspartate; AST, aspartate transaminase; Glc, glucose; Glu, glutamate; Mal, malate, MDH, malate dehydrogenase; OAA oxaloacetate; OGC, oxoglutarate carrier; OXPHOS, oxidative phosphorylation; Pyr, pyruvate; TCA, tricarboxylic acid.

with these observations, we have found that aspartate and glutamine levels are diminished in aralar-deficient retinas [33]. These results clearly show the importance of aralar in retinal metabolism of glucose and glutamine.

Another characteristic feature of the retina is the architecture of the photoreceptor synapse, known as "ribbon synapse" [37,38]. In this type of synapse, the presynaptic terminal encloses the postsynaptic terminals, so that the active zone is close to the receptors, and little glutamate spills out from it. The consequence is that most of the glutamate released is sequestered back to the photoreceptor, where the glutamate needs to be protected from oxidation so that the glutamate can be recycled back into synaptic vesicles [35,37-39]. In this scenario, a new role for aralar in the protection of glutamate from oxidation has recently been reported [35]. Normally aralar helps protect glutamate from oxidation. In the absence of aralar, glutamate levels decrease because synthesis of glutamine is impaired [33] and protection from oxidation is missing [35].

We have evaluated the impact of the metabolic alterations caused by aralar deficiency on the responses of the retina to light. We used ERG analysis to assess the functionality of diverse cell types in the retina [40]. Our results show that visual function is compromised in aralar-deficient mice, especially after a long period of dark-adaptation and in the recovery of responsitivity following a flash of light.

METHODS

Animals: All animal experiments were conducted in accordance with procedures approved in the Directive 86/609/EEC of the European Union, the Ethics Committee of the Universidad Autónoma de Madrid, and the Universidad de Alcalá and in accordance with the ARVO Statement for the Use of Animals in Ophthalmic and Vision Research. *Aralar/AGC1*$^{+/-}$ mice [31] were crossed to produce *Aralar/AGC1*$^{-/-}$ and A*ralar/AGC1*$^{+/+}$ control littermates in Dr. Jorgina Satrústegui's laboratory (Madrid, Spain) and bred with free access to water and a standard diet under a 12 h:12 h light-dark cycle (maximum 350 lux). Genotype was determined with PCR using genomic DNA from mice tails with the following primers: sense primer-a (mAra 3′-LTR-F3: 5′-GTT CTC TAG AAA CTG CTG AGG-3′) for mutated alleles, sense primer-b (mAra int-13F1: 5′-GAT GTG AGA ACT CAC CAG TGT-3′) for wild-type alleles, and antisense primer-c (mAra int-13B: 5′-ACC ACC ACC AGC GTG TCA GC-3′) for the mutant and wild-type alleles. PCR conditions were 35 cycles (94 ºC, 1 min; 58 ºC, 1 min; and 72 ºC, 1 min) for DNA amplication in a 25 µl mixture containing 200 ng DNA, 0.5 units Go Taq ® G2 Flexi DNA polymerase (Promega Biotech Ibérica, Alcobendas, Spain); 0.4 microMolar primers, 0.8 mM dideoxynucleotide Mix (Niborlab, Sevilla, Spain) and 2 mM $MgCl_2$ (Promega Biotech Ibérica, Alcobendas, Spain). Mutant (406 bp) and wild-type (271 bp) fragments were separated by electrophoresis on a 2% agarose gel [31].

Immunohistochemistry: Light-adapted animals were euthanized with cervical dislocation. The eyes were marked for orientation, fixed for 2 h in 4% paraformaldehyde (PFA), and embedded in optimum cutting temperature (Tissue-Tek®-OCT™; Sakura Tinetek Europe, Zoeterwoude, Netherlands; frozen sections) or fixed overnight in formalin and included in paraffin before slicing in the horizontal plane (nasal-temporal orientation). Paraffin-embedded sections (5 µm) were stained with hematoxylin and eosin for morphometric analysis. Briefly, retinal thickness was measured as the outer segment (OS), outer nuclear layer (ONL), inner nuclear layer (INL), and inner plexiform layer (IPL) length along the horizontal plane at approximate 450 µm intervals from the optic nerve head (ONH) toward the periphery with ImageJ. For inmunohistochemistry, retinal frozen sections (15 µm) were blocked (0.2% Triton X-100, 2% serum in PBS: 1X: 136 mM NaCl, 8 mM Na_2HPO_4, 2.68 mM KCl, 1.96 mM KH_2PO_4, pH 7.4).) for 1 h before overnight incubation with the indicated antibodies (Appendix 1). Antibody was washed, and the retinal sections were incubated with the appropriate secondary antibodies (Appendix 1) and 4',6-diamidino-2-phenylindole (DAPI) as the nuclear marker. Autofluorescence was quenched with Sudan Black treatment. Images were obtained at 40X magnification in a Leica TCS-SP5 microscope. The number of cells was estimated as nuclear counts (DAPI) in rows in the ONL and the INL and along the ganglion cell layer. The perimeter was measured along the outer plexiform layer (OPL) with ImageJ. Reagents were obtained from Sigma-Aldrich (Madrid, Spain) unless otherwise specified.

ERG recordings: Dark-adapted (>12 h) animals were anaesthetized with an intraperitoneal injection of saline solution (NaCl 0.9%), containing ketamine (70 mg/kg; Ketalar, Parke-Davis, Wellington, New Zealand) and xylazine (7 mg/kg; Rompun, Bayer, Leverkusen, Germany), and before recording, the pupils were dilated with one to two drops of 1% tropicamide (Alcon Cusí S.A., El Masnou, Barcelona, Spain). To preserve the corneal surface from desiccation, a drop of 2% methyl-cellulose was applied (Methocel, Ciba Vision, Hetlingen, Switzerland). Three recording electrodes (ground, reference, and corneal) were used (Burian-Allen, Hansen Ophthalmic Development Lab, Coralville, IA). The corneal electrode (contact lens type) was placed in the visual axis 5 mm from the cornea. In all experiments, animal

handling was performed under indirect dim red light (>620 nm) followed by 5 min in complete darkness before the recordings. Mice were kept at 37 °C on a heating pad (Hot-Cold, Pelton Shepherd Industries, Stockton, CA) during the entire procedure. Full-field ERG was the technique of choice. For low-intensity (<−2 log Cds/m^2) stimuli, a Ganzfeld dome, which ensures homogeneous illumination of at least 120° in the central retina, was used, whereas for higher-intensity stimuli (>−2 log Cds/m^2), a single light-emitting diode was placed close to the eye. The recorded electrophysiological response was amplified and filtered (CP511 AC amplifier; Grass Instruments, Quincy, MA), and digitalized (ADInstruments Ltd, Oxfordshire, UK). The whole process was controlled with Scope version 3.8.1 software (Power Lab, ADInstruments Ltd) [41,42]. The stimulation protocols were designed according to the International Society for Clinical Electrophysiology of Vision [43]. Six types of standard ERG responses were recorded with the protocols described in Appendix 2. Dim scotopic response (DSR), rod (b-scot), mixed (a-wave and b-wave), and oscillatory potential (OP) responses were recorded sequentially under dark background conditions, and cones (b-phot) and flicker responses were recorded following 5 min light-adaptation with background white light (50 Cd/m^2). To test the effect of reducing metabolic stress by illumination, animals were light-adapted for 5 min (50 Cd/m^2), and then the scotopic mixed response was recorded at different times in scotopic conditions. To test the effect of aralar absence on inner retinal cells, two identical saturating light flashes were applied with inter-stimulus of 0.3, 0.5, 1, and 2 s (double flash), with the protocol described for the mixed response. In those experiments, the mixed response in the overnight dark-adapted conditions was first acquired for each animal and used for normalization.

The DSR and rod response amplitudes were measured from baseline to the peak from the scotopic recordings; the a-wave amplitude was measured from baseline to the first trough from the mixed response or to the response amplitudes at 3 and 8 msec (in Appendix 3), and the b-wave and cone response amplitudes from the first trough to the peak from the mixed (b-wave) and photopic (b-phot) responses. OP and flicker were determined as the maximum amplitude between the trough and the peak of the waves.

Statistical analysis: Data are presented as mean ± standard error of the mean (SEM) of both eyes averaged per animal (n). The significance of the differences between genotypes was determined with unpaired two-tailed Student *t* tests or ANOVA followed by Bonferroni's test. A p value of less than 0.05 was considered statistically significant.

RESULTS

Aralar-deficient retinas have normal morphology and architecture: We first performed histological analysis of the control and aralar-deficient retinas (Figure 2, Figure 3) to evaluate the possibility of degeneration or under-development in aralar-deficient mice. Figure 2 shows the characteristic hematoxylin and eosin staining of the typical control (Figure 2A-D) and aralar-deficient retinas (Figure 2E-H) at 17 days old. The distribution and length of the layers were not altered by the absence of aralar (compare the images in the top and bottom rows in Figure 2 and in the corresponding histograms, Figure 2I-L).

The photoreceptors are the retinal cells that first respond to light. Therefore, the number of photoreceptors will have an impact on retinal activity. We found no differences in the photoreceptor outer segment length (Figure 2I) or in the photoreceptor distribution (Figure 3A-C,G-I) or numbers (Figure 3M). Similarly, the distribution of the inner retinal cells (Figure 3D-F,J-L) was unaltered as was the number of bipolar cells (Figure 3M) and ganglion cells (datanot shown). Furthermore, the number of pyknotic nuclei (less than 3–5%) was similar in both genotypes (data not shown). Mass spectrometry analysis of metabolites showed similar levels of taurine and cGMP (Figure 3N), two metabolites present mostly in photoreceptors. Eye size estimated from the retinal perimeter along the outer plexiform layer (Figure 3O,P) also was unchanged.

Dark-adapted ERG responses are diminished in photoreceptors from aralar-deficient mice: Next, we used electroretinography to analyze retinal cell function in aralar-deficient mice and in control siblings after overnight dark-adaptation (Figure 4). ERG waveforms obtained in scotopic (dark) and photopic (with background light) conditions in response to different light intensities can be used to study the behavior of the different retinal cells. Therefore, we recorded the electrical response to light after overnight dark-adaptation to increasing light flashes first in scotopic conditions and then in photopic conditions. Figure 4A shows the responses to dim (DSR), low (b-scot), and high-intensity (mixed) light flashes acquired in darkness. The responses mainly correspond to the activity of ganglion and amacrine cells, rod bipolar cells, and the whole retina [40,42]. The mixed response can be separated in the a-wave (initial downward response) that corresponds to the activity of the rods and cones followed by the upward response of the inner retina cells (b-wave). The b-wave can be filtered to obtain the OP that reflects the activity of ganglion cells and amacrine cells [40,42]. Aralar-deficient retinas show light-evoked ERG activity, but the ERG wave amplitude is reduced by half (non-significant decrease by 42±10.23%

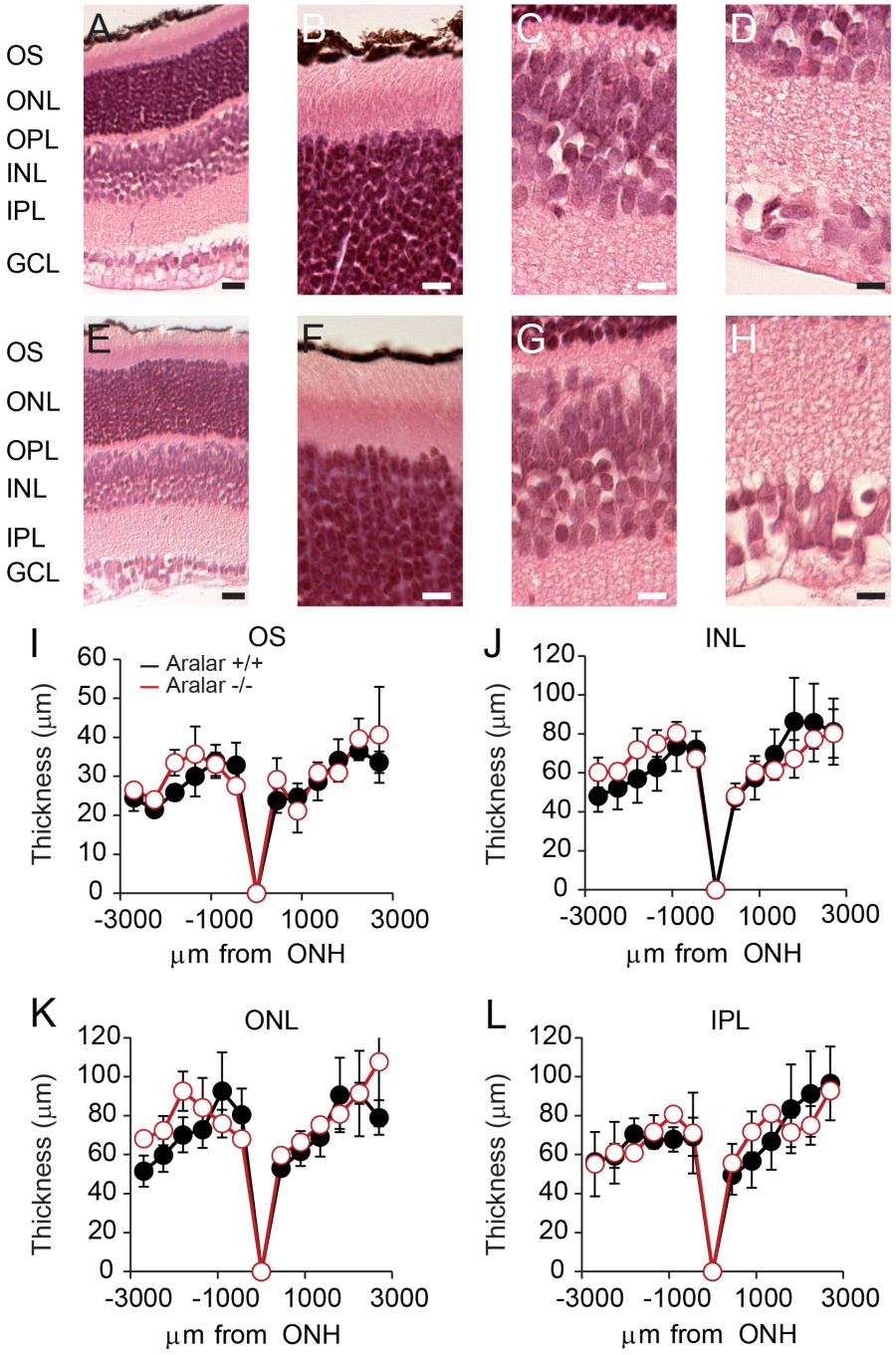

Figure 2. Morphological analysis of the retina shows no differences between the control and aralar-deficient retinas. Hematoxylin and eosin staining of control (**A**) and aralar-deficient (**E**) retinas. Scale bar = 100 µm. Insets correspond to the enlarged outer segment (OS), the outer nuclear layer (ONL; **B**, **F**), outer plexiform (OPL), inner nuclear layers (INL; **C**, **G**), inner plexiform (IPL), and granule cell layers (GCL; **D**, **H**). Scale bar = 10 µm. **I-L**: Histograms of measured thickness of the indicated layers along the optic nerve head meridian. (n = 3 for control and n = 3 for aralar-deficient retinas). (Student's t test).

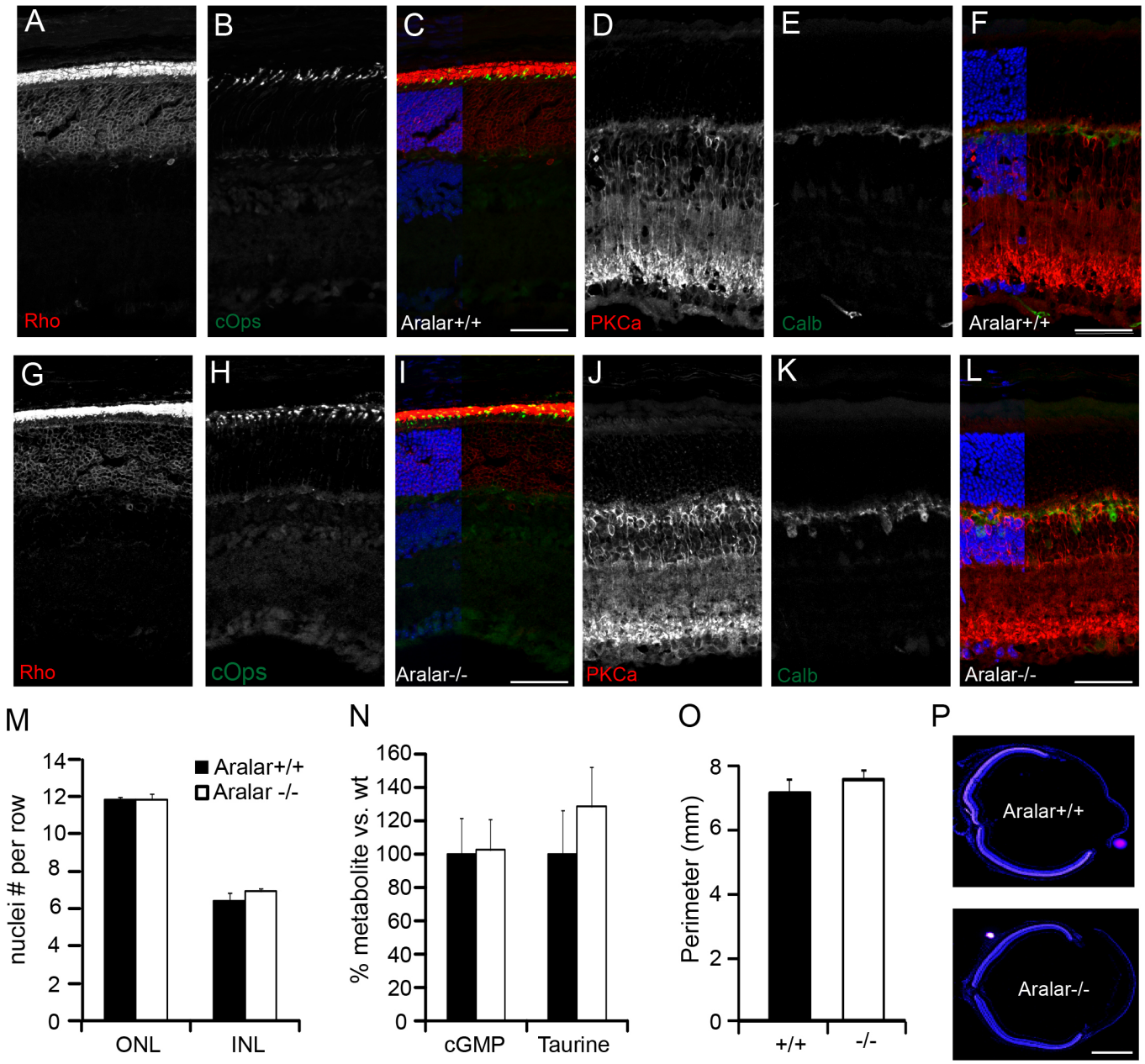

Figure 3. Cellular distribution is normal in aralar-deficient retinas. Fixed retinas from control (**A**-**F**) and aralar-deficient (**G**-**L**) mice (n = 3 each genotype, three independent assays) were probed with antibodies against rhodopsin (**A**, **G**), c-Opsin (**B**, **H**), protein kinase C alpha (PKC-α; **D**, **J**), and calbindin (**E**, **K**), which label the rods, cones, rod bipolar cells, and horizontal (as well as some amacrine and displaced amacrine) cells, respectively [67,68]. Nuclei stained with 4',6-diamidino-2-phenylindole (DAPI) are shown in blue in the merged images (**C**, **F**, **I**, **L**). Scale bar = 50 µm. **M**: Photoreceptor and inner retinal neuron density was estimated by counting the number of nuclei in rows at intervals from the optic nerve head (ONH) to the periphery (three rows of nuclei from three different sections from three animals per genotype). **N**: Taurine and cGMP levels from control (n = 6) and aralar-deficient (n = 8) retinas. Retinas were isolated in light conditions and processed as described previously [33,35] for metabolite extraction and gas chromatography/mass spectrometry analysis. Note that there are no significant differences between genotypes. **O**: Measured retinal size as the perimeter along the outer plexiform layer of the control and aralar-deficient mice as shown in **P**. Scale bar = 1 mm. Data are shown as mean ± standard error of the mean (SEM); n = 3. No significant difference between genotypes was found. (Student's t test).

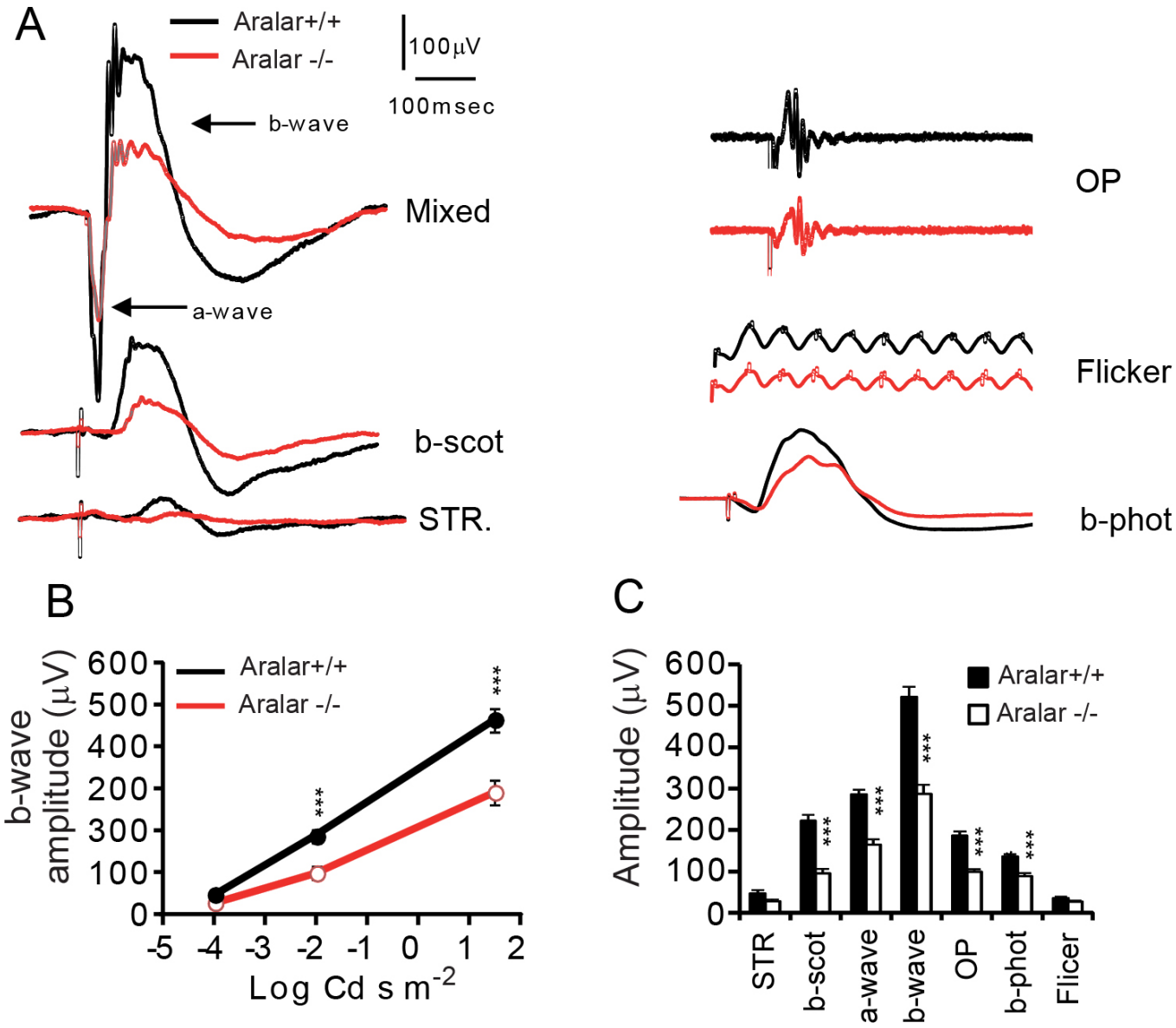

Figure 4. Aralar-deficient retinas show decreased light-evoked response after overnight dark-adaptation. Standard electroretinogram (ERG) representative trace recordings from control (black line) and aralar-deficient (red line) overnight dark-adapted animals. See for comparison the differences between the two genotypes in the trace amplitudes. Dim scotopic response (DSR, −4 log Cds/m^2), rod response (b-scot, −2 log Cds/m^2), rod and cone response (mixed, a- and b-waves, 1.5 log Cds/m^2), and oscillatory potential (OP, 1.5 log Cds/m^2) were recorded sequentially under scotopic conditions, i.e., a dark background. Cone (b-phot, 2 log Cds/m^2) and flicker (2 log Cds/m^2) responses were recorded after 5 min light-adaptation under photopic conditions, i.e., light background. Note that the OP and flicker responses were separated in the vertical axis to better present the genotype's waveform. **B**: B-wave amplitude in scotopic conditions at the different flash intensities. **C**: Histogram representation of the ERG wave amplitudes from the knockout (white bars) and control (black bars) animals. Wave amplitudes were averaged from a total of seven (**A**, **E**, **F**) and 12 (**B**, **C**, **D**) mice from each genotype. Data are shown as mean ± standard error of the mean (SEM); *** p<0.00001, **, p<0.0001, * p<0.01 for statistically significant differences between the genotypes (n = 7-12 each genotype).

Table 1. Calculated ERG parameters from aralar wt and KO retinas.

Genotype	ratio b/a	ratio DSR/b	Sensitivity (log Cd sm^{-2})	a-wave initial slope (µV/sec)	Implicit time (msec)	
					b-wave	b-phot
Aralar+/+	1.83±0.01	0.097±0.01	- 3.9±0.09	35.78±20.50	14.42±0.39	16.09±.43
Aralar −/−	1.82±0.21	0.102±0.02	- 3.6±0.12	18.46±15.17**	18.82±2.68*	20.96±0.43**
%	99.76	105.26	93%	51.61	130.52	130.29

b- to a-wave ratio and DSR to b-wave ratio, a-wave slope and implicit times were calculated from data of experiments presented in Figure 4 and are expressed as mean±SEM. Initial a-wave slope was calculated as maximal slope in the first 5 msec of downward response. Flash intensity required to elicit a 10% of maximal response (sensitivity) was interpolated from a dot-plot of DSR, b-scot and b- wave amplitudes versus the corresponding flash intensity (Figure 4B); and implicit times were measured as the time to reach half maximal upward amplitude from the first trough. Student *t* test of wt (n=7) versus KO (n=7) for statistical significance: * $p<0.05$; ** $p<0.005$.

in DSR; and significant decreases by 57±6.5%, b-scot; 42±5.43%, a-wave; 45±5.35%, b-wave; 44±7.17%, OP) at the different light intensities (Figure 4B) when compared to that of the control mice. The amplitude of the a-wave of the aralar-deficient retinas was decreased at the trough (Figure 4C) but also at 3 and 8 msec after the end of the flash pulse (Appendix 3), when there was still no bipolar cell activation, excluding an undue contribution of the altered b-wave initiation. The implicit times (time to reach half-maximal response of the b-wave) and the initial photoreceptor response (the a-wave initial slope) also were altered (Table 1). Furthermore, the flash intensity to elicit a 10% maximal response was similar in the aralar-deficient mice when compared with the control mice (Table 1, Figure 4B). We also calculated the b- to a-wave ratios and the DSR to b-wave ratios and found no differences between genotypes (Table 1), which points to photoreceptors as the primary affected cells.

Next, we tested the response to light in photopic conditions, when the rod response is saturated, to isolate the cone response. We found a decrease in the response amplitudes in the aralar-deficient retinas for single (b-phot, 42±4.2%) and high-frequency (flicker, 26.4±7.16%, statistically insignificant) stimulation (Figure 4A,C). In summary, our results show that aralar-deficient mice, although not blind [44], have a significant visual deficiency that appears to originate in photoreceptors.

Light-adaptation counteracts the impairment of responses in aralar-deficient retinas: Based on the critical role played by aralar in glucose oxidative metabolism [25,27], we hypothesized that the diminished photoreceptor responses in aralar-deficient retinas reflect the impairment of the energy production needed to maintain the dark current and glutamate vesicle recycling in darkness. Because light reduces the ATP demand of retinas [5], we reasoned that illumination would decrease metabolic stress and improve performance during subsequent ERG recordings in scotopic conditions.

To test this, we dark-adapted mice overnight and then illuminated them for 5 min (background white light, 50 Cd/m^2). This exposure to illumination decreased the ERG amplitude (Figure 5A), due to rhodopsin bleaching and desensitization. The ERG response then recovers over the next hour (Figure 5C,D). In the aralar-deficient retinas (Figure 5B), there is almost no effect on amplitude just after the 5 min illumination (Figure 5C,D), and the following recovery is more efficient than in the control retinas (compare % recovery at each time point between genotypes in Figure 5E,F). This is consistent with an improved energetic state of the aralar-deficient retinas caused by the decreased metabolic workload during the illumination period.

Paired-flash test in aralar-deficient retinas unveils a reduction of bipolar cell response: Aralar is also expressed by neurons of the inner retina that may be similarly affected by a lack of aralar when facing an increase in energy demand. Furthermore, the synaptic transmission at the ribbon synapse in aralar-deficient retinas may be affected by the reported reduction in glutamine levels reflecting the impaired de novo synthesis [33] that adds to the diminished protection of glutamate from oxidation in the absence of aralar [32,35]. These metabolic alterations would affect the b-wave independently of the a-wave alteration.

To investigate this possibility, we measured the influence of aralar on the ERG inner retina component using a paired-flash stimulation protocol. This protocol has been used previously to study the recovery of a-wave or photoreceptor activity [45,46]. We extended the application of the technique to study the recovery of postsynaptic activity (b-wave). We reasoned that if glutamate recycling was impaired or the repolarization of bipolar cells delayed, the b-wave measured

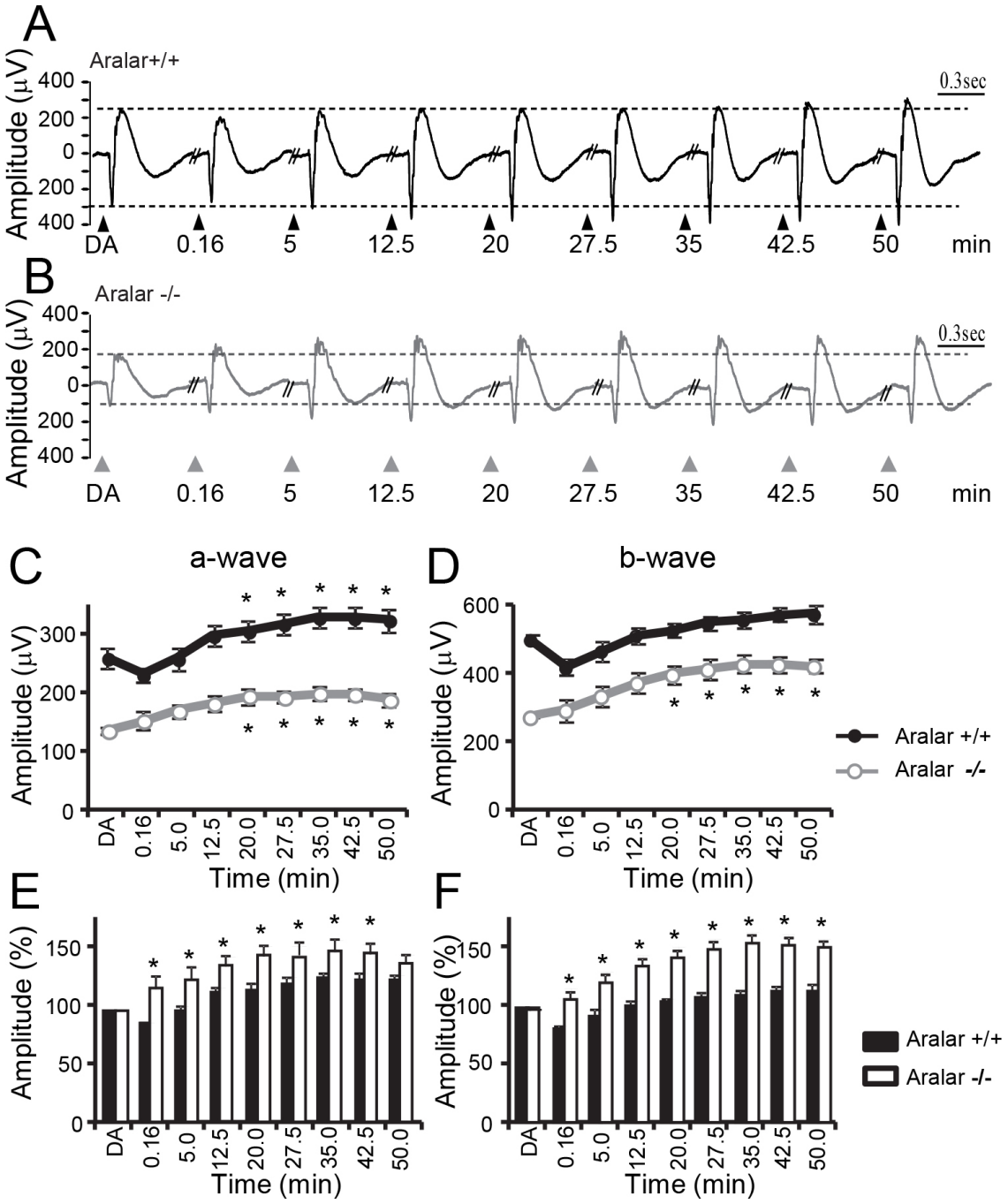

Figure 5. Aralar-deficient retinas recover faster after light illumination. Typical electroretinogram (ERG) mixed wave recordings from control (**A**) and knockout (**B**) mice obtained after overnight dark-adaptation (DA) and at different time points (0.16, 5, 12.5, 20, 27.5, 35, 42.5, and 50 min) after 5 min exposure to light. Measured amplitudes of a-wave (**C**) and b-wave (**D**) of control (black, filled circles) and knockout mice (gray, white circles) for full dark-adapted (DA) or at the indicated time points after light exposure. * $p<0.05$, statistically significant difference with dark-adapted amplitude. **E**, **F**: Corresponding histograms of normalized amplitudes to dark-adapted (DA) values. * $p<0.05$, statistically significant difference between genotypes. Data are expressed as mean ± standard error of the mean (SEM) of n = 7 (control) and n = 4 (knockout) mice.

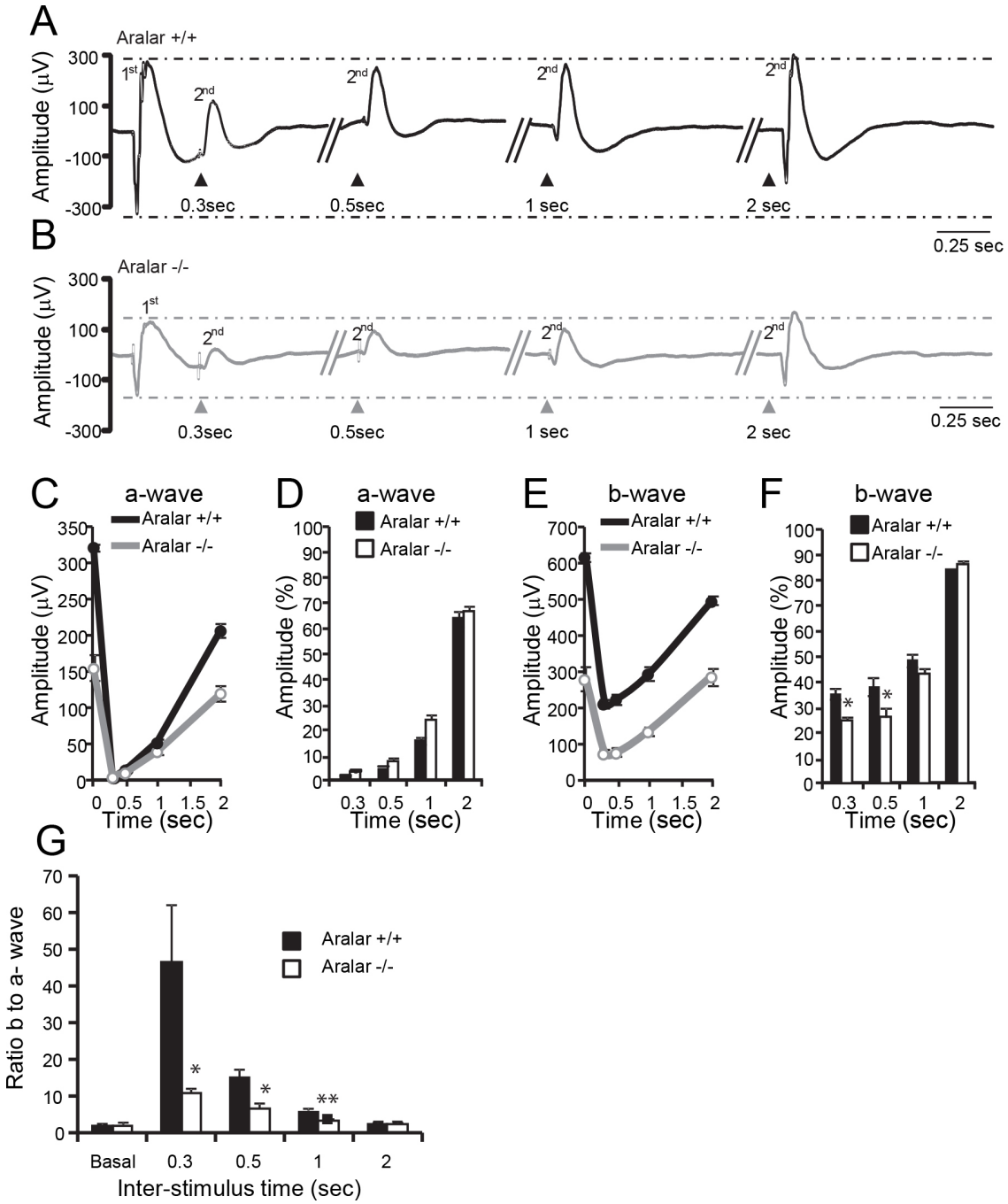

Figure 6. Aralar-deficient mice have a reduced rate of recovery in the double flash test. Typical electroretinogram (ERG) traces of the control (**A**) and knockout (**B**) paired-flash stimulation with the indicated time intervals for the second flash (the first flash of the paired stimulation is shown only for the first recording [leftmost]). The flash intensity was 1.5 log Cds/m^2 in scotopic conditions (the mixed protocol from Appendix 2). Amplitude (μV) versus the interval time plot of the second flash a-wave (**C**) and b-wave (**E**) for the control (black) and knockout (gray) mice. **D**, **F**: Corresponding histograms showing % values of the respective single flash amplitude. **G**: Calculated b-wave to a-wave ratio in the second flash ERG response at the different intervals. Basal refers to the initial single flash recording. * $p<0.05$; ** $p<0.005$ for statistical difference between genotypes (the Student *t* test). Data are expressed as mean ± standard error of the mean (SEM) of n = 4 (control) and n = 5 (knockout) mice.

in a second flash should show a further decrease in the aralar-deficient mice readily observable as a decrease in the b- to a-wave ratios.

In the control retinas (Figure 6A), the first flash abolishes the photoreceptor response (a-wave) for the second flash at the shortest interval times, but the second flash gradually recovers to 70% of the initial value at the longer interval time employed (Figure 6C,D). The decrease in the photoreceptor response is mirrored by a decrease to about 40% of the inner retina response (b-wave), which recovers to 90% of the initial value (Figure 6E,F). In the aralar-deficient retinas (Figure 6B), the a-wave, although reduced in amplitude, recovers with a similar time course as the control retinas (Figure 6C,D). This is consistent with the reported normal levels of phototransduction proteins in aralar-deficient mice [35]. However, the b-wave decrease is bigger than in the controls at shorter time intervals (25% and 26% in the aralar-deficient retinas versus 35% and 38% in the control retinas at 0.3 and 0.5 s, respectively, Figure 6F). To account for the contribution of the first flash recovery to the second one, especially at the shortest inter-stimulus time, we subtracted the single flash waveform from that of the double flash (Appendix 4) and found a similar reduction in the b-wave amplitude in aralar-deficient retinas. We also found a slight increase in the a-wave amplitude at short times (0.3–1 s, Figure 6C) in the aralar-deficient retinas that is likely due to the delayed b-mixed wave initiation and would not explain the strikingly different b- to a-wave ratio behavior between genotypes (Figure 6G).

DISCUSSION

Aralar-deficient retinas are morphologically normal but have reduced dark-adapted ERG response: Photoreceptor degeneration is a leading cause of blindness [47]. The decrease in ERG amplitude we observed also occurs in retinal degeneration models where the retina cell numbers are decreased [41,42,48,49]. However, this is not always the case as in other animal models such as monocarboxylate transporter 3 knockout [50], carbonic anhydrase knockout [51] and in hypoglycemia [20] or in early stages of diabetes [52], a decrease in ERG amplitudes was observed before cell loss.

The results shown in Figure 2 and Figure 3 are consistent with previous findings of similar levels of rhodopsin, recoverin, and COX1, major markers of photoreceptor development, in aralar-deficient retinas [35]. The results are also in accordance with the absence of neurodegeneration in the central nervous system, as observed with cresyl violet staining [31] and NeuN immunolabeling [53] in the brain of aralar-deficient mice. Thus, a decrease in photoreceptor numbers as the explanation for the reduced amplitude of ERG waves is not at the basis of the reported phenotype, at least at the age under examination that is near the survival limit for these knockout animals.

Photoreceptors have high levels of aralar [34] and other MAS components [54], contain about 55–65% of retinal mitochondria [8], and are among the most metabolically demanding types of cells, energetically and from the point of view of glutamate homeostasis. Given the role of aralar in glucose oxidative metabolism [25,27], glutamine de novo synthesis [33], and glutamate homeostasis [35], photoreceptors would be the type of cell that is most likely to be affected by aralar genetic ablation.

Signal transmission in the retina is vertical from first-order neurons (photoreceptors) to second- and third-order neurons (bipolar and ganglion cells, respectively), so any defect in photoreceptor activity also will affect responses from the following layers of cells, with a certain gain relationship between two adjacent cell layers [40]. We found a decrease in all ERG wave elements (Figure 4) in the aralar-deficient retinas, but the fact that the ratio of waves corresponding to adjacent layers is maintained between genotypes (b- to a-mixed, DSR to b-mixed, Table 1) indicates that photoreceptors are the cells primarily affected by aralar deficiency.

Illumination partly rescues the effect: Aralar deficiency in retinas increases the lactate to pyruvate ratio by twofold [35]. The deficiency also diminishes incorporation of ^{13}C from ^{13}C-glucose into tricarboxylic acid cycle intermediates in isolated retinas [36]. These findings are consistent with an inefficient supply of pyruvate to mitochondria, as also occurs in cultured neurons [27]. Although retinas are highly glycolytic [4,6], some glucose is oxidized in mitochondria, and its metabolism increases in darkness when the energy demand is higher [4-6,8,17]. The diminished oxidative metabolism of glucose in aralar-deficient retinas may contribute to a state of diminished energy production and slower dark current and vesicle recycling. The deficiency would have its greatest impact after a long period of high metabolic demand, such as overnight dark-adaptation. The consequence would be the lower light-evoked ERG amplitude responses that we observed under those conditions (Figure 4). Illumination decreases the metabolic stress and allows the recovery of aralar-deficient retinas that return more efficiently to preillumination response values than the control counterparts (Figure 5). The light-induced decrease in the ERG response in photopic versus scotopic conditions is similar in both genotypes (reduction by 69±1.33% versus 66±2.7% of b-phot compared with b-mixed wave in control and aralar-deficient retinas, Figure 4) and argues against incomplete light adaptation as an explanation for the improved response at the

shortest time point in aralar-deficient retinas. Although the involvement of other factors [55] in the "super-recovery" of aralar-deficient retinas after illumination cannot be excluded, the immediacy of the super-response is consistent with the role of the reversal of metabolic stress in the aralar-deficient retina.

In normal retinas, the recovery of the ERG response to dark-adapted levels is largely dependent on the amount of rhodopsin bleached by the adapting illumination [56,57]. Diabetic rats recover faster from light-adaptation than control animals, possibly because the diabetic animals have reduced levels of rhodopsin [58]. We do not expect this to be the case in aralar-deficient retinas, which have similar levels of rhodopsin and recoverin as the control retinas [35]. Interestingly, decreased levels of aralar [59], glutamine [60], and glutamate [61] synthesis have been reported in diabetic retinas.

Metabolic alteration of inner retina cells decreases b-wave: Another remarkable finding of our study is the substantial decrease in the second response in the paired-flash ERG analyses (Figure 6). This is consistent with a limitation in synaptic transmission that is reflected in the diminished responses of inner retinal cells (b-wave component; Figure 4). This could be due either to altered glutamate cycling, to an energy deficit of the inner retina neurons, or both (Figure 1).

Retinas have developed a system based on continuous glutamate release to the invaginated ribbon-type synapses that greatly improves the signal-to-noise ratio at the expense of the need for a high turnover of glutamate vesicles and ATP-consuming rates [38,62]. Light decreases the release rate, and thus, the glutamate concentration at the synaptic cleft reduces the saturation of the postsynaptic metabotropic receptors and depolarizing ON bipolar cells via a G-protein-mediated transduction pathway [38,63]. In the control retinas, glutamate is protected from oxidation [35] and stored back in vesicles at the photoreceptor synapse for the next release round. However, in aralar-deficient retinas, glutamate is less well protected from oxidative metabolism [35] and may be consumed oxidatively as an alternative fuel to compensate for impaired glucose utilization. Glutamine, a major glutamate precursor, also can be used as an oxidative substrate as shown by the partial recovery of the ERG amplitude in monocarboxylate transporter-inhibited retinas [22]. The impaired pathway for glutamine synthesis in these animals [33] further reduces glutamate availability. The consequence would be less glutamate to refill synaptic vesicles in photoreceptors and to fully saturate the postsynaptic receptors at the ribbon synapse. This is consistent with the reduced b-wave of the second flash in Figure 6. Pharmacological inhibition of glutamate availability with inhibitors of either glutamine synthetase or glutamate uptake [64-66] similarly affects the b-wave.

Although light hyperpolarizes photoreceptors and decreases their energetic burden [5], light has mixed effects on inner retina neurons. When the ON bipolar cells sense a decrease in glutamate, they depolarize and experience increased ATP demand to fuel the ion pumps that repolarize them (Figure 1). In cultured neurons, the aralar-MAS pathway activates mitochondrial metabolism in response to an increased workload [27]. Therefore, ON bipolar cells that are deficient in aralar may fail to increase energy production to match the increased workload caused by light. This would delay repolarization so that the ON bipolar neurons do not respond efficiently to a second flash. The reduced b- to a-wave ratio in aralar-deficient retinas (Figure 6G) is consistent with impairment of glutamate recycling and with an energy deficit within ON bipolar cells.

Conclusions: In this report, we have shown that aralar deficiency alters the response of the retina to light. The reduced light-evoked amplitude of ERGs is not associated with decreased cell numbers but can be traced back to the known effect of aralar on glucose and glutamine and glutamate metabolism. Our findings suggest that there could be a previously missed visual phenotype associated with the aralar-MAS deficiency in humans with global cerebral hypomyelination (OMIM 612949).

APPENDIX 1. LIST OF ANTIBODIES.

To access the data, click or select the words "Appendix 1."

APPENDIX 2. ERG PROTOCOL SETTINGS.

To access the data, click or select the words "Appendix 2."

APPENDIX 3. A-WAVE AMPLITUDE IS REDUCED IN ARALAR DEFICIENT RETINAS.

To access the data, click or select the words "Appendix 3." A-wave amplitude was measured from baseline at 3, 8 and 15 msec of the end of the stimulus. The reduction in amplitude is similar at 3 and 8 msec, when no b-wave contribution is present and at 15 msec, which is near the trough. Data are mean± standard error of the mean (SEM), *** $p<0.01$ (ANOVA followed by Bonferroni's test).

APPENDIX 4. CORRECTION OF SINGLE FLASH TRAIL AT 0.3 AND 0.5 SEC INTERVAL FOR PAIRED FLASH.

To access the data, click or select the words "Appendix 4." Typical traces of control (A) and aralar-deficient (B) mice of single flash (black), paired flashes with 0.3 and 0.5 sec interval (gray) and the result of subtracting the single flash from the paired flashes (red). (C) a-wave and (D) b-wave amplitude normalized (%) to single flash amplitude values respectively. Data are mean± standard error of the mean (SEM), * $p<0.05$ (ANOVA followed by Bonferroni's test).

ACKNOWLEDGMENTS

This work was supported by grants BFU201-30456-C02-01/BMC and SAF2014-56929R from Ministerio de Economía y Competitividad and S2010/BMD-2402 from Comunidad Autónoma de Madrid (to JS), FIS-RD12-0034-0006 and PI13–02098 from Instituto de Salud Carlos III (to PdlV), EY06641 and EY017863 from the National Institutes of Health (to JBH) and an institutional grant from Fundación Areces to the Centro de Biología Molecular Severo Ochoa. LC has been recipient of a Junta de Ampliación de Estudios-Consejo Superior de Investigaciones Científicas and CIBERER postdoctoral contracts. The authors declare no competing financial interests.

REFERENCES

1. Wong-Riley MT. Energy metabolism of the visual system. Eye Brain 2010; 2:99-116. [PMID: 23226947].
2. Ames A 3rd. Energy requirements of CNS cells as related to their function and to their vulnerability to ischemia: a commentary based on studies on retina. Can J Physiol Pharmacol 1992; 70:SupplS158-64. [PMID: 1295666].
3. Webvision: The Organization of the Retina and Visual System Kolb H FE, Nelson R, editor. Salt Lake City (UT): University of Utah Health Sciences Center; 1995–2016.
4. Ames A 3rd, Li YY, Heher EC, Kimble CR. Energy metabolism of rabbit retina as related to function: high cost of Na+ transport. J Neurosci 1992; 12:840-53. [PMID: 1312136].
5. Okawa H, Sampath AP, Laughlin SB, Fain GL. ATP consumption by mammalian rod photoreceptors in darkness and in light. Curr Biol 2008; 18:1917-21. [PMID: 19084410].
6. Winkler BS. Glycolytic and oxidative metabolism in relation to retinal function. J Gen Physiol 1981; 77:667-92. [PMID: 6267165].
7. Winkler BS, Starnes CA, Twardy BS, Brault D, Taylor RC. Nuclear magnetic resonance and biochemical measurements of glucose utilization in the cone-dominant ground squirrel retina. Invest Ophthalmol Vis Sci 2008; 49:4613-9. [PMID: 18566456].
8. Medrano CJ, Fox DA. Oxygen consumption in the rat outer and inner retina: light- and pharmacologically-induced inhibition. Exp Eye Res 1995; 61:273-84. [PMID: 7556491].
9. Wang L, Tornquist P, Bill A. Glucose metabolism of the inner retina in pigs in darkness and light. Acta Physiol Scand 1997; 160:71-4. [PMID: 9179313].
10. Wang L, Tornquist P, Bill A. Glucose metabolism in pig outer retina in light and darkness. Acta Physiol Scand 1997; 160:75-81. [PMID: 9179314].
11. Ahmed J, Braun RD, Dunn R Jr, Linsenmeier RA. Oxygen distribution in the macaque retina. Invest Ophthalmol Vis Sci 1993; 34:516-21. [PMID: 8449672].
12. Kimble EA, Svoboda RA, Ostroy SE. Oxygen consumption and ATP changes of the vertebrate photoreceptor. Exp Eye Res 1980; 31:271-88. [PMID: 6968685].
13. Linsenmeier RA. Effects of light and darkness on oxygen distribution and consumption in the cat retina. J Gen Physiol 1986; 88:521-42. [PMID: 3783124].
14. Linsenmeier RA, Braun RD. Oxygen distribution and consumption in the cat retina during normoxia and hypoxemia. J Gen Physiol 1992; 99:177-97. [PMID: 1613482].
15. Poitry S, Tsacopoulos M, Fein A, Cornwall MC. Kinetics of oxygen consumption and light-induced changes of nucleotides in solitary rod photoreceptors. J Gen Physiol 1996; 108:75-87. [PMID: 8854338].
16. Zuckerman R, Weiter JJ. Oxygen transport in the bullfrog retina. Exp Eye Res 1980; 30:117-27. [PMID: 6968271].
17. Du J, Rountree A, Cleghorn WM, Contreras L, Lindsay KJ, Sadilek M, Gu H, Djukovic D, Raftery D, Satrustegui J, Kanow M, Chan L, Tsang SH, Sweet IR, Hurley JB. Phototransduction Influences Metabolic Flux and Nucleotide Metabolism in Mouse Retina. J Biol Chem 2016; 291:4698-710. [PMID: 26677218].
18. Bui BV, Kalloniatis M, Vingrys AJ. The contribution of glycolytic and oxidative pathways to retinal photoreceptor function. Invest Ophthalmol Vis Sci 2003; 44:2708-15. [PMID: 12766077].
19. Holfort SK, Klemp K, Kofoed PK, Sander B, Larsen M. Scotopic electrophysiology of the retina during transient hyperglycemia in type 2 diabetes. Invest Ophthalmol Vis Sci 2010; 51:2790-4. [PMID: 20042648].
20. Umino Y, Everhart D, Solessio E, Cusato K, Pan JC, Nguyen TH, Brown ET, Hafler R, Frio BA, Knox BE, Engbretson GA, Haeri M, Cui L, Glenn AS, Charron MJ, Barlow RB. Hypoglycemia leads to age-related loss of vision. Proc Natl Acad Sci USA 2006; 103:19541-5. [PMID: 17159157].
21. Winkler BS. Relative inhibitory effects of ATP depletion, ouabain and calcium on retinal photoreceptors. Exp Eye Res 1983; 36:581-94. [PMID: 6852134].
22. Bui BV, Kalloniatis M, Vingrys AJ. Retinal function loss after monocarboxylate transport inhibition. Invest Ophthalmol Vis Sci 2004; 45:584-93. [PMID: 14744902].

23. Noell WK. The effect of iodoacetate on the vertebrate retina. J Cell Physiol 1951; 37:283-307. [PMID: 14832350].

24. del Arco A, Satrustegui J. Molecular cloning of Aralar, a new member of the mitochondrial carrier superfamily that binds calcium and is present in human muscle and brain. J Biol Chem 1998; 273:23327-34. [PMID: 9722566].

25. Satrustegui J, Pardo B, Del Arco A. Mitochondrial transporters as novel targets for intracellular calcium signaling. Physiol Rev 2007; 87:29-67. [PMID: 17237342].

26. Pardo B, Rodrigues TB, Contreras L, Garzon M, Llorente-Folch I, Kobayashi K, Saheki T, Cerdan S, Satrustegui J. Brain glutamine synthesis requires neuronal-born aspartate as amino donor for glial glutamate formation. J Cereb Blood Flow Metab 2011; 31:90-101. [PMID: 20736955].

27. Llorente-Folch I, Rueda CB, Amigo I, del Arco A, Saheki T, Pardo B, Satrustegui J. Calcium-regulation of mitochondrial respiration maintains ATP homeostasis and requires ARALAR/AGC1-malate aspartate shuttle in intact cortical neurons. J Neurosci. 2013;33(35):13957–71, 71a.

28. Pardo B, Contreras L, Serrano A, Ramos M, Kobayashi K, Iijima M, Saheki T, Satrustegui J. Essential role of aralar in the transduction of small Ca2+ signals to neuronal mitochondria. J Biol Chem 2006; 281:1039-47. [PMID: 16269409].

29. Contreras L, Gomez-Puertas P, Iijima M, Kobayashi K, Saheki T, Satrustegui J. Ca2+ Activation kinetics of the two aspartate-glutamate mitochondrial carriers, aralar and citrin: role in the heart malate-aspartate NADH shuttle. J Biol Chem 2007; 282:7098-106. [PMID: 17213189].

30. Contreras L, Satrustegui J. Calcium signaling in brain mitochondria: interplay of malate aspartate NADH shuttle and calcium uniporter/mitochondrial dehydrogenase pathways. J Biol Chem 2009; 284:7091-9. [PMID: 19129175].

31. Jalil MA, Begum L, Contreras L, Pardo B, Iijima M, Li MX, Ramos M, Marmol P, Horiuchi M, Shimotsu K, Nakagawa S, Okubo A, Sameshima M, Isashiki Y, Del Arco A, Kobayashi K, Satrustegui J, Saheki T. Reduced N-Acetylaspartate Levels in Mice Lacking Aralar, a Brain- and Muscle-type Mitochondrial Aspartate-glutamate Carrier. J Biol Chem 2005; 280:31333-9. [PMID: 15987682].

32. Hurley JB, Chertov AO, Lindsay K, Giamarco M, Cleghorn W, Du J, Brockerhoff S. Energy Metabolism in the Vertebrate Retina In: Furakawa T, Hurley, J.B., Kawamura, S., editor. Vertebrate Photoreceptor Functional Molecular Bases: Springer; 2014. p. 91–138.

33. Lindsay KJ, Du J, Sloat SR, Contreras L, Linton JD, Turner SJ, Sadilek M, Satrustegui J, Hurley JB. Pyruvate kinase and aspartate-glutamate carrier distributions reveal key metabolic links between neurons and glia in retina. Proceedings of the National Academy of Sciences of the United States of America. 2014;111(43):15579–84. Epub 2014/10/15.

34. Xu Y, Ola MS, Berkich DA, Gardner TW, Barber AJ, Palmieri F, Hutson SM, LaNoue KF. Energy sources for glutamate neurotransmission in the retina: absence of the aspartate/glutamate carrier produces reliance on glycolysis in glia. J Neurochem 2007; 101:120-31. [PMID: 17394462].

35. Du J, Cleghorn W, Contreras L, Linton JD, Chan GC, Chertov AO, Saheki T, Govindaraju V, Sadilek M, Satrustegui J, Hurley JB. Cytosolic reducing power preserves glutamate in retina. Proceedings of the National Academy of Sciences of the United States of America. 2013;110(46):18501–6. Epub 2013/10/16.

36. Du J, Cleghorn WM, Contreras L, Lindsay K, Rountree AM, Chertov AO, Turner SJ, Sahaboglu A, Linton J, Sadilek M, Satrustegui J, Sweet IR, Paquet-Durand F, Hurley JB. Inhibition of mitochondrial pyruvate transport by zaprinast causes massive accumulation of aspartate at the expense of glutamate in the retina. J Biol Chem 2013; 288:36129-40. [PMID: 24187136].

37. Rao-Mirotznik R, Harkins AB, Buchsbaum G, Sterling P. Mammalian rod terminal: architecture of a binary synapse. Neuron 1995; 14:561-9. [PMID: 7695902].

38. Singer JH. Multivesicular release and saturation of glutamatergic signalling at retinal ribbon synapses. J Physiol 2007; 580:23-9. [PMID: 17218359].

39. Hasegawa J, Obara T, Tanaka K, Tachibana M. High-density presynaptic transporters are required for glutamate removal from the first visual synapse. Neuron 2006; 50:63-7. [PMID: 16600856].

40. Nguyen CT, Vingrys AJ, Wong VH, Bui BV. Identifying cell class specific losses from serially generated electroretinogram components. BioMed Res Int. 2013; 2013:796362-[PMID: 24089688].

41. Barhoum R, Martinez-Navarrete G, Corrochano S, Germain F, Fernandez-Sanchez L, de la Rosa EJ, de la Villa P, Cuenca N. Functional and structural modifications during retinal degeneration in the rd10 mouse. Neuroscience 2008; 155:698-713. [PMID: 18639614].

42. Germain F, Istillarte M, Gomez-Vicente V, Perez-Rico C, de la Villa P. Electroretinographical and histological study of mouse retina after optic nerve section: a comparison between wild-type and retinal degeneration 1 mice. Clin Experiment Ophthalmol 2013; 41:593-602. [PMID: 23279351].

43. Marmor MF, Fulton AB, Holder GE, Miyake Y, Brigell M, Bach M. ISCEV Standard for full-field clinical electroretinography (2008 update). Doc Ophthalmol 2009; 118:69-77. [PMID: 19030905].

44. Llorente-Folch I, Sahun I, Contreras L, Casarejos MJ, Grau JM, Saheki T, Mena MA, Satrustegui J, Dierssen M, Pardo B. AGC1-malate aspartate shuttle activity is critical for dopamine handling in the nigrostriatal pathway. J Neurochem 2013; 124:347-62. [PMID: 23216354].

45. Kang Derwent JJ, Saszik SM, Maeda H, Little DM, Pardue MT, Frishman LJ, Pepperberg DR. Test of the paired-flash electroretinographic method in mice lacking b-waves. Vis Neurosci 2007; 24:141-9. [PMID: 17640404].

46. Pennesi ME, Howes KA, Baehr W, Wu SM. Guanylate cyclase-activating protein (GCAP) 1 rescues cone recovery kinetics in GCAP1/GCAP2 knockout mice. Proceedings of the National Academy of Sciences of the United States of America. 2003;100(11):6783–8. Epub 2003/05/07.

47. Punzo C, Xiong W, Cepko CL. Loss of daylight vision in retinal degeneration: are oxidative stress and metabolic dysregulation to blame? J Biol Chem 2012; 287:1642-8. [PMID: 22074929].

48. Chang B, Hawes NL, Hurd RE, Davisson MT, Nusinowitz S, Heckenlively JR. Retinal degeneration mutants in the mouse. Vision Res 2002; 42:517-25. [PMID: 11853768].

49. Gao J, Cheon K, Nusinowitz S, Liu Q, Bei D, Atkins K, Azimi A, Daiger SP, Farber DB, Heckenlively JR, Pierce EA, Sullivan LS, Zuo J. Progressive photoreceptor degeneration, outer segment dysplasia, and rhodopsin mislocalization in mice with targeted disruption of the retinitis pigmentosa-1 (Rpl) gene. Proceedings of the National Academy of Sciences of the United States of America. 2002;99(8):5698–703. Epub 2002/04/18.

50. Daniele LL, Sauer B, Gallagher SM, Pugh EN Jr, Philp NJ. Altered visual function in monocarboxylate transporter 3 (Slc16a8) knockout mice. Am J Physiol Cell Physiol 2008; 295:C451-7. [PMID: 18524945].

51. Ogilvie JM, Ohlemiller KK, Shah GN, Ulmasov B, Becker TA, Waheed A, Hennig AK, Lukasiewicz PD, Sly WS. Carbonic anhydrase XIV deficiency produces a functional defect in the retinal light response. Proceedings of the National Academy of Sciences of the United States of America. 2007;104(20):8514–9. Epub 2007/05/09.

52. Phipps JA, Fletcher EL, Vingrys AJ. Paired-flash identification of rod and cone dysfunction in the diabetic rat. Invest Ophthalmol Vis Sci 2004; 45:4592-600. [PMID: 15557472].

53. Ramos M, Pardo B, Llorente-Folch I, Saheki T, Del Arco A, Satrustegui J. Deficiency of the mitochondrial transporter of aspartate/glutamate aralar/AGC1 causes hypomyelination and neuronal defects unrelated to myelin deficits in mouse brain. J Neurosci Res 2011; 89:2008-17. [PMID: 21608011].

54. Ross CD, Godfrey DA. Distributions of aspartate aminotransferase and malate dehydrogenase activities in rat retinal layers. J Histochem Cytochem 1985; 33:624-30. .

55. McKeown AS, Kraft TW. Adaptive potentiation in rod photoreceptors after light exposure. J Gen Physiol 2014; 143:733-43. [PMID: 24821966].

56. Kang Derwent JJ, Qtaishat NM, Pepperberg DR. Excitation and desensitization of mouse rod photoreceptors in vivo following bright adapting light. J Physiol 2002; 541:201-18. [PMID: 12015430].

57. Lee KA, Nawrot M, Garwin GG, Saari JC, Hurley JB. Relationships among visual cycle retinoids, rhodopsin phosphorylation, and phototransduction in mouse eyes during light and dark adaptation. Biochemistry 2010; 49:2454-63. [PMID: 20155952].

58. Phipps JA, Yee P, Fletcher EL, Vingrys AJ. Rod photoreceptor dysfunction in diabetes: activation, deactivation, and dark adaptation. Invest Ophthalmol Vis Sci 2006; 47:3187-94. [PMID: 16799066].

59. Zhong Q, Kowluru RA. Diabetic retinopathy and damage to mitochondrial structure and transport machinery. Invest Ophthalmol Vis Sci 2011; 52:8739-46. [PMID: 22003103].

60. Lieth E, LaNoue KF, Antonetti DA, Ratz M. Diabetes reduces glutamate oxidation and glutamine synthesis in the retina. The Penn State Retina Research Group. Exp Eye Res 2000; 70:723-30. [PMID: 10843776].

61. Gowda K, Zinnanti WJ, LaNoue KF. The influence of diabetes on glutamate metabolism in retinas. J Neurochem 2011; 117:309-20. [PMID: 21288239].

62. Linton JD, Holzhausen LC, Babai N, Song H, Miyagishima KJ, Stearns GW, Lindsay K, Wei J, Chertov AO, Peters TA, Caffe R, Pluk H, Seeliger MW, Tanimoto N, Fong K, Bolton L, Kuok DL, Sweet IR, Bartoletti TM, Radu RA, Travis GH, Zagotta WN, Townes-Anderson E, Parker E, Van der Zee CE, Sampath AP, Sokolov M, Thoreson WB, Hurley JB. Flow of energy in the outer retina in darkness and in light. Proceedings of the National Academy of Sciences of the United States of America. 2010;107(19):8599–604. Epub 2010/05/07.

63. Schneider FM, Mohr F, Behrendt M, Oberwinkler J. Properties and functions of TRPM1 channels in the dendritic tips of retinal ON-bipolar cells. Eur J Cell Biol 2015; 94:420-7. [PMID: 26111660].

64. Barnett NL, Pow DV, Robinson SR. Inhibition of Muller cell glutamine synthetase rapidly impairs the retinal response to light. Glia 2000; 30:64-73. [PMID: 10696145].

65. Bui BV, Hu RG, Acosta ML, Donaldson P, Vingrys AJ, Kalloniatis M. Glutamate metabolic pathways and retinal function. J Neurochem 2009; 111:589-99. [PMID: 19702659].

66. Winkler BS, Kapousta-Bruneau N, Arnold MJ, Green DG. Effects of inhibiting glutamine synthetase and blocking glutamate uptake on b-wave generation in the isolated rat retina. Vis Neurosci 1999; 16:345-53. [PMID: 10367968].

67. Haverkamp S, Wassle H. Immunocytochemical analysis of the mouse retina. J Comp Neurol 2000; 424:1-23. [PMID: 10888735].

68. de la Villa P, Kurahashi T, Kaneko A. L-glutamate-induced responses and cGMP-activated channels in three subtypes of retinal bipolar cells dissociated from the cat. J Neurosci 1995; 15:3571-82. [PMID: 7538564].

Articles are provided courtesy of Emory University and the Zhongshan Ophthalmic Center, Sun Yat-sen University, P.R. China. The print version of this article was created on 12 October 2016. This reflects all typographical corrections and errata to the article through that date. Details of any changes may be found in the online version of the article.